

Fusion barrier distribution and superheavy elements

K. Hagino^{1,2} and T. Tanaka^{3,4}

¹ Department of Physics, Tohoku University, Sendai 980-8578, Japan

² Research Center for Electron Photon Science, Tohoku University, 1-2-1 Mikamine, Sendai 982-0826, Japan

³ RIKEN Nishina Center for Accelerator-Based Science, Saitama 351-0198, Japan

⁴ Department of Physics, Kyushu University, Fukuoka 819-0395, Japan

Abstract. The barrier distribution, originated from channel coupling effects in heavy-ion fusion reactions, has been extracted experimentally for many systems using either a fusion excitation function or an excitation function of large-angle quasi-elastic scattering. In this article, we discuss an application of the latter method to the $^{48}\text{Ca}+^{248}\text{Cm}$ system, which is relevant to hot fusion reactions to synthesize superheavy elements. To this end, we carry out coupled-channels calculations for this system, taking into account the deformation of the target nucleus, and discuss the role of deformation in a formation of evaporation residues.

1. Introduction

Fusion reactions play an important role in several phenomena in physics. Those include the energy production in stars, nucleosyntheses, and formations of superheavy elements. Yet, from the theoretical point of view, fusion reactions, as well as fission, are typical examples of large amplitude collective motions of quantum many-body systems, and their microscopic understanding has still been far from complete.

In order to understand the dynamics of nuclear fusion, the Coulomb barrier between two nuclei plays an important role. This is a potential barrier formed as a result of cancellation between the long-ranged repulsive Coulomb interaction and a short ranged attractive nuclear interaction. The height of the Coulomb barrier defines the energy scale of a system, and here in this article, we shall mainly consider the energy region around the Coulomb barrier.

It has by now been well known that heavy-ion fusion cross sections are largely enhanced at energies below the Coulomb barrier, as compared to a prediction of a simple potential model. It has been understood that channel coupling effects, that is, the couplings of the relative motion between two nuclei to several collective excitations of the colliding nuclei, as well as particle transfer channels, play an essential role in enhancing subbarrier fusion cross sections [1, 2, 3, 4, 5]. The coupled-channels approach has been developed in order to take into account such channel coupling effects [6].

In the eigen-channel representation of the coupled-channels method, fusion cross sections in the presence of channel couplings can be represented as a weighted sum of fusion cross sections for each eigen-channel [7]. In this picture, a single Coulomb barrier is replaced by a distribution of multitude of barriers due to the channel coupling effects. A way to extract the barrier distribution directly from experimental fusion cross sections has been proposed by Rowley, Satchler, and Stelson [8]. In this method, the barrier distribution is extracted by taking the second energy derivative of the product of fusion cross sections, σ_{fus} , and incident energies

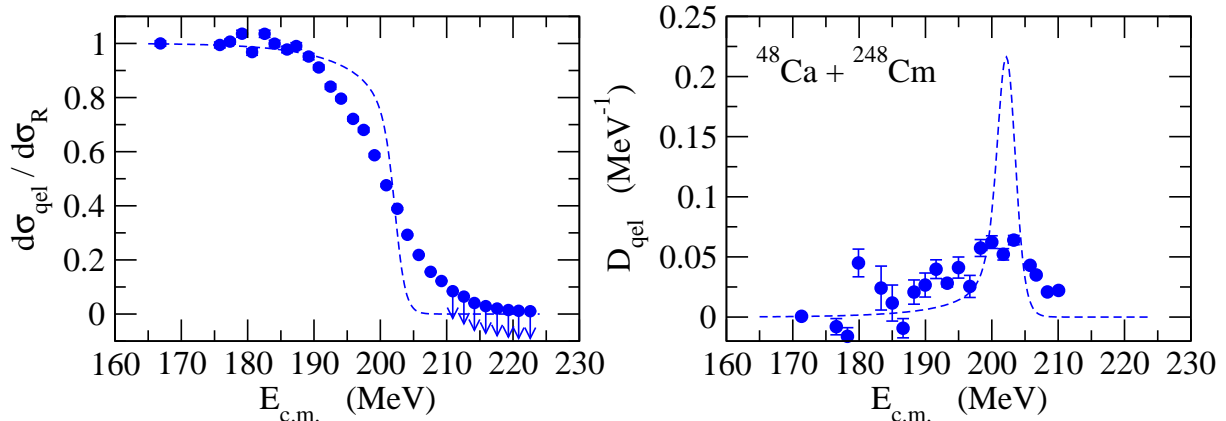


Figure 1. The quasi-elastic cross sections (the left panel) and the corresponding barrier distribution (the right panel) for the $^{48}\text{Ca}+^{248}\text{Cm}$ system. The experimental data are shown by the filled circles, where the arrows indicate the upper limit of cross sections. For comparison, the result of a potential model calculation is also shown by the dashed lines. The experimental data are taken from Ref. [14].

in the center of mass frame, E , that is, $d^2(E\sigma_{\text{fus}})/dE^2$. The fusion barrier distribution has been extracted with this method for many systems [2, 9], which in general show that the shape of barrier distribution is sensitive to details of channel couplings, thus providing a good tool to understand the underlying dynamics of subbarrier fusion reactions.

It has been shown that a similar barrier distribution can be obtained also by using quasi-elastic scattering at backward angles [10, 11]. This is because quasi-elastic scattering corresponds to a reflection of flux at the barrier and thus it is complementary to fusion, which corresponds to a transmission of flux through the barrier. Very recently, the quasi-elastic barrier distribution was extracted for the $^{48}\text{Ca}+^{248}\text{Cm}$ system [14], the system which had been used to synthesize superheavy elements $Z = 116$ (Lv) [12, 13]. Using the GARIS ion separator at RIKEN, which has been used to synthesize the $Z = 113$ element (Nihonium) [17], quasi-elastic cross sections have been successfully measured, which are almost free from contamination of deep-inelastic cross sections. The barrier distribution extracted from such data is thus much better defined as compared to the previous attempts [15, 16] for systems relevant to the superheavy nuclei.

In this article, in order to discuss the reaction dynamics for superheavy elements, we present the coupled-channels analyses for the quasi-elastic barrier distribution for the $^{48}\text{Ca}+^{248}\text{Cm}$ system [14]. We consider the deformation of the target nucleus, ^{248}Cm , as well as a neutron transfer channel. We also discuss the connection of the barrier distribution to the measured evaporation residue cross sections.

2. Quasi-elastic barrier distribution

Quasi-elastic scattering is defined as a sum of elastic, inelastic, transfer, and breakup processes. That is, it is an inclusive process, being complementary to fusion. The quasi-elastic barrier distribution, D_{qel} , is defined as [10, 11],

$$D_{\text{qel}}(E) = -\frac{d}{dE} \left(\frac{\sigma_{\text{qel}}(E, \pi)}{\sigma_R(E, \pi)} \right), \quad (1)$$

where $\sigma_{\text{qel}}(E, \pi)$ is a quasi-elastic cross section at the scattering angle π and $\sigma_R(E, \pi)$ is the Rutherford cross section. In previous measurements, quasi-elastic scattering was measured by

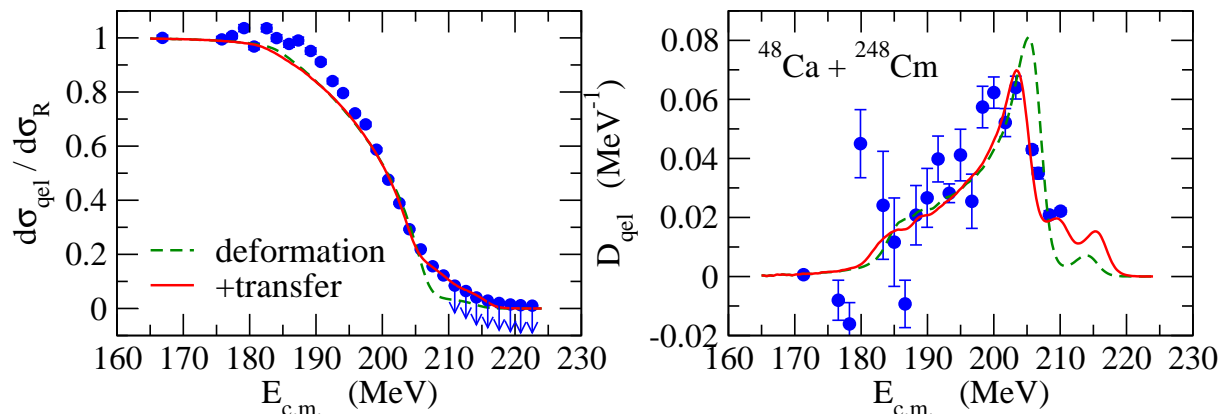


Figure 2. The quasi-elastic cross sections (the left panel) and the barrier distribution (the right panel) for the $^{48}\text{Ca}+^{248}\text{Cm}$ system. The dashed lines show the result of coupled-channels calculations which take into account the deformation of the target nucleus, ^{248}Cm , as well as the octupole phonon excitation in the projectile nucleus, ^{48}Ca . The solid lines are obtained by including in addition the neutron transfer channel. The experimental data are taken from Ref. [14].

detecting projectile-like particles at the scattering angle θ (in the center of mass frame) and the cross sections were mapped on those at $\theta = \pi$ using the effective energy defined by [10, 11],

$$E_{\text{eff}} = 2E \frac{\sin(\theta/2)}{1 + \sin(\theta/2)}. \quad (2)$$

The mapping has been shown to work well as long as the scattering angle θ is close to π [11]. In the new measurement with GARIS, on the other hand, the recoiled target-like particles were measured at π and the mapping of the quasi-elastic cross sections was not required [14]. This was not possible in the previous measurements, as it would have required to put a detector along the beam line. The measured quasi-elastic cross sections and the corresponding barrier distribution are shown in Fig. 1. The filled circles with arrows indicate the upper limit of cross sections, for which the deep-inelastic component may contaminate to some extent. For comparison, the figure also shows the result of a potential model. To this end, we use a Woods-Saxon potential with the depth parameter of $V_0 = -105$ MeV, the range parameter of $r_0 = 1.18$ fm, and the surface diffuseness parameter of $a = 0.6$ fm. The imaginary part of the potential is set to be well localized inside the barrier. It is clearly seen that the experimental barrier distribution is much more structured as compared to the result of the potential model, indicating the importance of channel coupling effects.

3. Coupled-channels calculations for the $^{48}\text{Ca}+^{248}\text{Cm}$ system

Let us then perform coupled-channels calculations and discuss the role of channel coupling effects, in particular the role of deformation of the target nucleus, ^{248}Cm . For a well deformed nucleus, for which the excitation energies of the ground state rotational band are small, cross sections for quasi-elastic scattering can be computed as [11],

$$\frac{d\sigma_{\text{qel}}}{d\Omega} = \sum_I \frac{d\sigma_I}{d\Omega} = \int_0^1 d(\cos\theta) \left(\frac{d\sigma_{\text{el}}}{d\Omega} \right)_\theta, \quad (3)$$

where σ_I is the cross section to populate the state with spin I in the ground state rotational band (including the ground state with $I = 0$). $(d\sigma_{el}/d\Omega)_\theta$ is the cross section for elastic scattering for a fixed orientation angle θ for the target nucleus. This is calculated with a deformed potential for each θ , $V(r, \theta)$, where r is the relative distance between the two colliding nuclei. Notice that in this approximation the coupled-channels equations are completely decoupled and the cross sections are given as a weighted sum of cross sections for a single-channel system labeled by θ (for which there are only elastic scattering and absorption).

The dashed lines in Fig. 2 show the result of a coupled-channels calculation so obtained. To this end, we use the deformation parameters of $\beta_2 = 0.297$ and $\beta_4 = 0.04$ together with the radius parameter of $R_T = 1.2 \times 248^{1/3}$ fm [18]. We also take into account the octupole vibrational excitation in ^{48}Ca at 4.51 MeV with the (dynamical) deformation parameter of $\beta_3 = 0.175$, although the excitation energy is large and the excitation simply renormalizes the internucleus potential [3, 19]. One can see that a large part of the structure in the barrier distribution is well reproduced by this calculation. Especially, the asymmetric shape of the barrier distribution is well accounted for.

A further improvement can be achieved by taking into account the neutron transfer channel. The solid lines in Fig. 2 show the results with the 1 neutron pick-up channel, whose ground-state-to-ground-state Q value is $Q_{gg} = -1.06$ MeV. We adjust the coupling strength for the transfer channel in order to reproduce the experimental quasi-elastic cross sections. This calculation slightly improves the cross sections around $E = 210$ MeV, and the main peak in the barrier distribution is somewhat altered. However, the modification is minor, and one can conclude that the main effect still comes from the deformation of the target nucleus.

4. Connection to evaporation residue formations

The barrier distribution discussed in the previous sections provides information on the Coulomb barrier in the entrance channel, that is, before the colliding nuclei reach the touching configuration. For medium-heavy systems, a compound nucleus is formed almost automatically once the touching configuration is achieved [3]. In contrast, in the superheavy region, there is a huge probability for the touching configuration to re-separate without forming a compound nucleus, that is, quasi-fission, due to a strong Coulomb repulsion between the two nuclei. Furthermore, even if a compound nucleus is formed with a small probability, it decays most likely by fission. Because quasi-fission characteristics significantly overlap with fission of the compound nucleus, a detection of fission events itself does not guarantee a formation of the compound nucleus. Therefore, a formation of superheavy elements is usually identified by detecting evaporation residues. A question then arises: what is the connection between the barrier distribution in the entrance channel and evaporation residue cross sections?

Figure 3 answers this question. This figure compares the quasi-elastic barrier distribution with the measured evaporation residue cross sections for the $^{48}\text{Ca}+^{248}\text{Cm}$ system. For the barrier distribution, the figure also shows the result of the coupled-channels calculation (the solid line). The contribution of the side collision ($\theta = \pi/2$) is denoted by the dashed curve. The figure clearly indicates that the maximum of the evaporation residue cross sections originates from the side collision. This is a clear confirmation of the notion of compactness proposed by Hinde *et al.* [20], who argued that the side collision leads to a compact touching configuration, for which the effective barrier height for the diffusion process is low, enhancing the formation probability of a compound nucleus.

This notion has further been confirmed theoretically using an extended version of the fusion-by-diffusion model [18]. The fusion-by-diffusion model is a simple one-dimensional model for the diffusion process proposed by Swiatecki *et al.* [21, 22, 23]. In this model, the potential for the diffusion process is parameterized as a parabolic function of s , that is the surface separation between the two spheres. Assuming the overdamped limit, the diffusion probability, P_{CN} , is

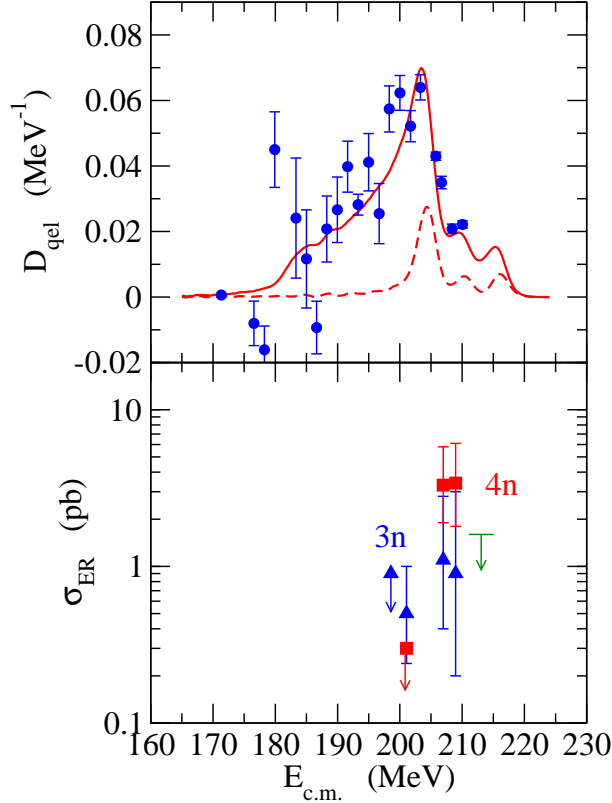


Figure 3. The experimental quasi-elastic barrier distribution (the upper panel) and the evaporation residue cross sections (the lower panel) for the $^{48}\text{Ca}+^{248}\text{Cm}$ system. For the barrier distribution, the figure also shows the results of the coupled-channels calculation (the solid line), for which the contribution of the side collision ($\theta = \pi/2$) is denoted by the dashed line. The experimental data are taken from Refs. [12, 13, 14].

then computed as [24],

$$P_{\text{CN}} = \frac{1}{2} \left[1 - \text{erf} \left(\sqrt{\frac{\Delta V}{T}} \right) \right], \quad (4)$$

where $\text{erf}(x)$ is the error function, T is the temperature of the system, and $\Delta V = V_{\text{fiss}}(s_{\text{sd}}) - V_{\text{fiss}}(s_{\text{inj}})$ is the difference between the potential energy at the saddle configuration, s_{sd} , and that at the injection point, s_{inj} . In the fusion-by-diffusion model, the fission potential, $V_{\text{fiss}}(s)$, as well as the saddle configuration, s_{sd} , are globally parameterized according to Refs. [21, 22, 23], and the injection point, s_{inj} , is treated as an adjustable parameter. In Ref. [18], this model has been extended by introducing the angle dependence to the injection point as,

$$s_{\text{inj}}(\theta) = s_{\text{inj}}^{(0)} + R_T \sum_{\lambda} \beta_{\lambda T} Y_{\lambda 0}(\theta). \quad (5)$$

The solid lines in Fig. 4 show the evaporation residue cross sections for the $^{48}\text{Ca}+^{248}\text{Cm}$ system obtained with this model [18]. The contributions of the side ($\theta = \pi/2$) and the tip ($\theta = 0$) collisions are denoted by the dashed and the dotted lines, respectively. At energies around 211 MeV, that is, the energies slightly above the barrier height for the side collision (see Fig. 3), the side collision gives the main contribution. At these energies, the contribution of the tip

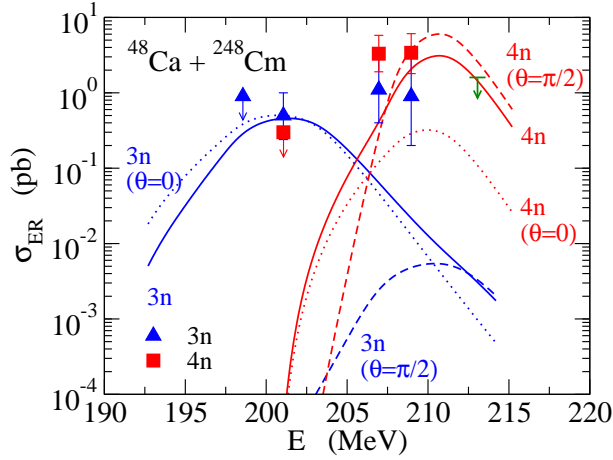


Figure 4. The evaporation residue cross sections for the $^{48}\text{Ca}+^{248}\text{Cm}$ system obtained with the extended fusion-by-diffusion model. The solid lines show the orientation averaged cross sections, while the dotted and the dashed lines denote the contributions of the tip ($\theta = 0$) and the side ($\theta = \pi/2$) collisions, respectively. The experimental data are taken from Refs. [12, 13].

collision is much smaller, since the injection point is large, and thus the diffusion probability is small. On the other hand, the side collision is largely suppressed at lower energies due to the small capture probability originated from a high capture barrier. The contribution of the tip collision then becomes dominant, for which the capture probability is not suppressed, even though the diffusion probability is small. In this way, the maximum of the evaporation residue cross sections are obtained at energies slightly above the barrier height for the side collision, at which the energy is high enough so that the capture probability is not suppressed and at the same time one can take advantage of large diffusion probabilities for the side collision.

5. Summary

The fusion barrier distribution has provided useful information on the reaction dynamics for heavy-ion sub-barrier fusion reactions for many systems. This continues to be the case also for systems relevant to superheavy elements. In this article, we have discussed the quasi-elastic barrier distribution for the $^{48}\text{Ca}+^{248}\text{Cm}$ system, that is, the system to synthesize the element 116 (Lv) with hot fusion reaction. The coupled-channels analyses for the recently measured data have clearly indicated that the side collision plays an important role in forming evaporation residues and that the maximum of the evaporation residue cross sections appears at energies slightly above the height of the Coulomb barrier for the side collision. This has made a clear confirmation of the notion of compactness for the side collision, which has also been confirmed theoretically using the extended fusion-by-diffusion model.

Of course, there still remain many challenges in nuclear reaction studies for superheavy elements, such as a clarification of shape evolution towards a compound nucleus with a deformed target, a role of quantum friction, and to understand the reaction dynamics of neutron-rich nuclei [25]. Apparently much more theoretical and experimental works will be required in order to gain a deeper insight into reaction dynamics for superheavy elements.

Acknowledgments

The authors thank K. Morita for useful discussions. K.H. also thanks V. Guimarães for his hospitality during his stay in Sao Paulo.

References

- [1] A.B. Balantekin and N. Takigawa, *Rev. Mod. Phys.* **70**, 77 (1998).
- [2] M. Dasgupta, D.J. Hinde, N. Rowley, and A.M. Stefanini, *Annu. Rev. Nucl. Part. Sci.* **48**, 401 (1998).
- [3] K. Hagino and N. Takigawa, *Prog. Theor. Phys.* **128**, 1061 (2012).
- [4] B.B. Back, H. Esbensen, C.L. Jiang, and K.E. Rehm, *Rev. Mod. Phys.* **86**, 317 (2014).
- [5] G. Montagnoli and A.M. Stefanini, *Eur. Phys. J. A* **53**, 169 (2017).
- [6] K. Hagino, N. Rowley, and A.T. Kruppa, *Comp. Phys. Comm.* **123**, 143 (1999).
- [7] C.H. Dasso, S. Landowne, and A. Winther, *Nucl. Phys. A* **405**, 381 (1983); *Nucl. Phys. A* **407**, 221 (1983).
- [8] N. Rowley, G.R. Satchler, and P.H. Stelson, *Phys. Lett. B* **254**, 25 (1991).
- [9] J.R. Leigh, M. Dasgupta, D.J. Hinde, J.C. Mein, C.R. Morton, R.C. Lemmon, J.P. Lestone, J.O. Newton, H. Timmers, J.X. Wei, and N. Rowley, *Phys. Rev. C* **52**, 3151 (1995).
- [10] H. Timmers, J.R. Leigh, M. Dasgupta, D.J. Hinde, R.C. Lemmon, J.C. Mein, C.R. Morton, J.O. Newton, and N. Rowley, *Nucl. Phys. A* **584**, 190 (1995).
- [11] K. Hagino and N. Rowley, *Phys. Rev. C* **69**, 054610 (2004); *Brazilian J. of Phys.* **35**, 890 (2005).
- [12] Yu. Ts. Oganessian *et al.*, *Phys. Rev. C* **70**, 064609 (2004); *Phys. Rev. C* **63**, 011301 (2000).
- [13] S. Hofmann *et al.*, *Eur. Phys. J. A* **48**, 62 (2012).
- [14] T. Tanaka, Y. Narikiyo, K. Morita, K. Fujita, D. Kaji, K. Morimoto, S. Yamaki, Y. Wakabayashi, K. Tanaka, M. Takeyama, A. Yoneda, H. Haba, Y. Komori, S. Yanou, B.J.-P. Gall, Z. Asfari, H. Faure, H. Hasebe, M. Huang, J. Kanaya, M. Murakami, A. Yoshida, T. Yamaguchi, F. Tokanai, T. Yoshida, S. Yamamoto, Y. Yamano, K. Watanabe, S. Ishizawa, M. Asai, R. Aono, S. Goto, K. Katori, and K. Hagino, *J. Phys. Soc. Jpn.* **87**, 014201 (2018).
- [15] S. Mitsuoka *et al.*, *Phys. Rev. Lett.* **99**, 182701 (2007).
- [16] S.S. Ntshangase *et al.*, *Phys. Lett. B* **651**, 27 (2007).
- [17] K. Morita *et al.*, *J. of Phys. Soc. Jpn.* **73**, 2593 (2004); **76**, 5001 (2007); **81**, 3201 (2012).
- [18] K. Hagino, *Phys. Rev. C* **98**, 014607 (2018).
- [19] N. Takigawa, K. Hagino, M. Abe, and A.B. Balantekin, *Phys. Rev. C* **49**, 2630 (1994).
- [20] D.J. Hinde *et al.*, *Phys. Rev. Lett.* **74**, 1295 (1995).
- [21] W.J. Swiatecki, K. Siwek-Wilczynska, and J. Wilczynski, *Acta Phys. Pol. B* **34**, 2049 (2003).
- [22] W.J. Swiatecki, K. Siwek-Wilczynska, and J. Wilczynski, *Phys. Rev. C* **71**, 014602 (2005).
- [23] T. Cap, K. Siwek-Wilczynska, and J. Wilczynski, *Phys. Rev. C* **83**, 054602 (2011).
- [24] Y. Abe, D. Boilley, B.G. Giraud, and T. Wada, *Phys. Rev. E* **61**, 1125 (2000).
- [25] K. Hagino, arXiv: 1812.05805 [nucl-th].